Contrib Mineral Petrol (2007) 153:355–367
DOI 10.1007/s00410-006-0151-y

ORIGINAL PAPER

Cs-dominant polylithionite in the Koktokay#3 pegmatite, Altai, NW China: in situ micro-characterization and implication for the storage of radioactive cesium

R. C. Wang · H. Hu · A. C. Zhang · F. Fontan · Ph. de Parseval · S. Y. Jiang

Received: 21 December 2005 / Accepted: 26 September 2006 / Published online: 4 November 2006

Abstract Except forming two Cs-rich minerals like pollucite and londonite, cesium generally occurs in trace amounts in potassium-bearing minerals owing to its very low Clarke value and large ionic radius. However, in the Koktokay#3 pegmatite (Altai, NW China), lepidolite is extremely enriched in cesium (typically 21–26 wt% Cs_2O). Cs-enriched lepidolite is restricted to the inner of the pegmatite, where four types of occurrence are characterized by using in situ techniques (EMP: electron microprobe, micro-XRD: micro-area X-ray diffractometer and Raman probe: micro-area Raman spectrometer) as: (1) outer zones on Cs-poor lepidolite cores; (2) fine overgrowths on muscovite veinlets; (3) veinlets in Cs-poor lepidolite and (4) veinlets in elbaite. There is an inverse correlation between K and Cs and in terms of ^{VI}Al versus Cs/(K+Cs), the Cs-dominant micas are an analog of the Li-rich mica polylithionite. Micro-XRD patterns and micro-Raman spectra indicate that Cs-dominant polylithionite structurally corresponds to minerals of the lepidolite series. According to its distribution and compositional characteristics, the Cs-dominant polylithionite seems to have formed at the magmatic to hydrothermal transition stage of pegmatitic magma evolution as a result of marginal replacement of early-formed lepidolite by Cs-rich fluids. Alternatively, it may have formed through direct precipitation from Cs-rich fluids. The results of the present study have important implications for the storage of nuclear waste in that Li mica such as polylithionite is a good candidate for immobilizing high-level radioactive cesium waste.

Communicated by J. Hoefs.

R. C. Wang (✉) · H. Hu · A. C. Zhang · S. Y. Jiang
State Key Lab for Mineral Deposits Research, Department of Earth Sciences, Nanjing University, Nanjing 210093, China
e-mail: rcwang@nju.edu.cn

F. Fontan · Ph. de Parseval
LMTG-UMR 5563, Université Paul Sabatier, 14 avenue Edouard Belin, Toulouse 31400, France

Introduction

Cesium is a rare alkali element distinguished by its very low Clarke value (2 ppm, McDonough et al. 1992) and very large ionic radius (1.67 Å, Shannon 1976), and occurs in traces in potassium-bearing minerals. Pollucite and londonite are the two main Cs-rich minerals known in nature, where they occur in highly evolved granitic pegmatites. Micas can contain minor to substantial amounts of cesium. Examples of Cs-bearing mica include cesian biotite (Cs_2O = 5.97 wt%, Ginsburg et al. 1972) and rubidian cesian phlogopite (Cs_2O = 6.60 wt%, Hawthorne et al. 1999). Examples suggesting dominance of cesium in the interlayer sites of mica have been described by Černý et al. (1994) and Huang et al. (2002). Nanpingite (Cs_2O = 25.29 wt%, Yang et al. 1988) is the Cs analog of muscovite, but is only described from its type locality (Nanping rare-element granitic pegmatite in southern China). Černý et al. (2003) described the mode of occurrence and chemical composition of polylithionite, annite and phlogopite with Cs-dominant populations from the Red Cross Lake rare-element pegmatites in north-central Manitoba, Canada. Wang et al. (2004) also identified the Cs-dominant analog of polylithionite in

the Yichun topaz–lepidolite granite, southern China. However, many questions remain concerning notably the species of mica that preferably hosts Cs, and the conditions under which Cs-dominant micas crystallize in granitic or pegmatitic magmas.

From another viewpoint, micas have been proposed as promising candidates for storage of radiogenic Cs isotopes (Mellini et al. 1996). Ferruginous trioctahedral mica (e.g., ''Cs-tetra-ferri-annite'') is considered the most suitable phase to host Cs, which is easily synthesized under hydrothermal conditions (Drábek et al. 1998). However, the synthesis of Cs-rich lithian mica has not yet been reported previously and little is known about the substitution of cesium in the interlayer sites of lepidolite.

In the Koktokay#3 pegmatite (Altai, NW China), lepidolite is extremely enriched in cesium with Cs_2O contents between 21 and 26 wt%, in addition to pollucite as a major Cs mineral (Wang et al. 2006). Moreover, Cs-enriched lepidolite coexists with Cs-poor lepidolite or muscovite. The aims of the present study are to characterize on a micro-scale the Cs-dominant analog of lepidolite from this pegmatite using multiple in situ techniques (EMP: electron microprobe, micro-XRD: micro-area X-ray diffractometer and Raman probe: micro-area Raman spectrometer), to examine the amount of Cs in the interlayer sites of mica ranging from low-Cs to Cs-dominant lepidolite. We also discuss the implications of these results for the storage of radioactive cesium.

Geological setting of the Koktokay#3 pegmatite

The Koktokay#3 pegmatite is one of the thousands of pegmatite dykes in the Altai pegmatite district, NW China (Fig. 1a). According to Černý's (1991) classification, the Koktokay#3 pegmatite belongs to the spodumene-subtype category. In the past several decades, the pegmatite was mainly mined for spodumene, lepidolite, beryl, pollucite and columbite-tantalite, but mining activities ceased several years ago.

The characteristics of the Koktokay#3 pegmatite are discussed in an earlier publication (Zhang et al. 2004b) and here we present a simplified geological map (Fig. 1a) and another showing the distribution of nine mineral zones recognized in the pegmatite (Fig. 1b). Only zones V–VIII are mineralized in rare metals (Ta, Nb, Be, Li, Cs). Pollucite, one of the two principal carriers of cesium in the pegmatite, appears mostly in zones V, VI and VII (Wang et al. 2006), whereas Cs-rich lepidolite is more widespread in zones V, VI, VII and VIII.

In situ analytical methods

Electron microprobe

Polished thin sections were initially examined using the back-scattered electron (BSE) mode of a JEOL JXA8800 electron microprobe (EMP) in the Department of Earth Sciences, Nanjing University, in order to characterize the internal chemical heterogeneity of the Cs minerals. Mineral compositions were determined using the same instrument in wavelength–dispersion mode. The operating conditions were as follows: accelerated voltage 15 kV, beam current 20 nA, beam diameter 1 μm. Both natural and synthetic standards were used: Amelia albite (Na Lα), Tanco pollucite (Cs Kα, Al Lα, Si Lα), orthoclase (K Kα), amazonitic K-feldspar (Rb Lα), hornblende (Mg Lα, Fe Kα, Ca Kα), Durango fluorapatite (F Lα). The ZAF program was used for data reduction (Armstrong 1989). The lithium content of lepidolite was determined according to the empirical equation Li_2O (wt%) = (0.287 × SiO_2)–9.552 for the trioctahedral polylithionite and trilithionite (Tindle and Webb 1990), and according to the equation $Li_2O = 0.3935F^{1.326}$ for dioctahedral muscovite (Tischendorf et al. 1997).

Micro-area X-ray diffractometer

A polished thin section was used to investigate lepidolite using a Rigaku D/max-RAPID micro-area X-ray diffractometer (micro-XRD), in the X-ray Application Laboratory of Rigaku Corporation, Japan. To facilitate selection of the area for examination, a color CCD camera was used to view the specimen. The beam was collimated to 100 μm. Experimental conditions are X-ray target: Cu Kα; voltage: 40 kV; current: 36 mA; collimator: 0.03 mm; exposure time: 1 h; axes: ω fixed at 25°, ϕ fixed at 0° (Rigaku Corporation 1999).

Micro-area Raman spectrometer

Raman spectra were recorded at room temperature on polished thin sections with a Renishaw RM2000 Raman spectrometer equipped with a CCD detector, in the Department of Earth Sciences of Nanjing University with excitation laser wavelength of 514 nm (Ar^+ laser), laser energy of 5 mW, spectral slit of 25 μm and collecting time of 30 min. The 50 × objective was used on a Leica DM/LM microscope. With this objective, the lateral spot-size of the laser beam was about 1 μm. Silicon (520 cm^{-1} Raman shift) was used as a standard.

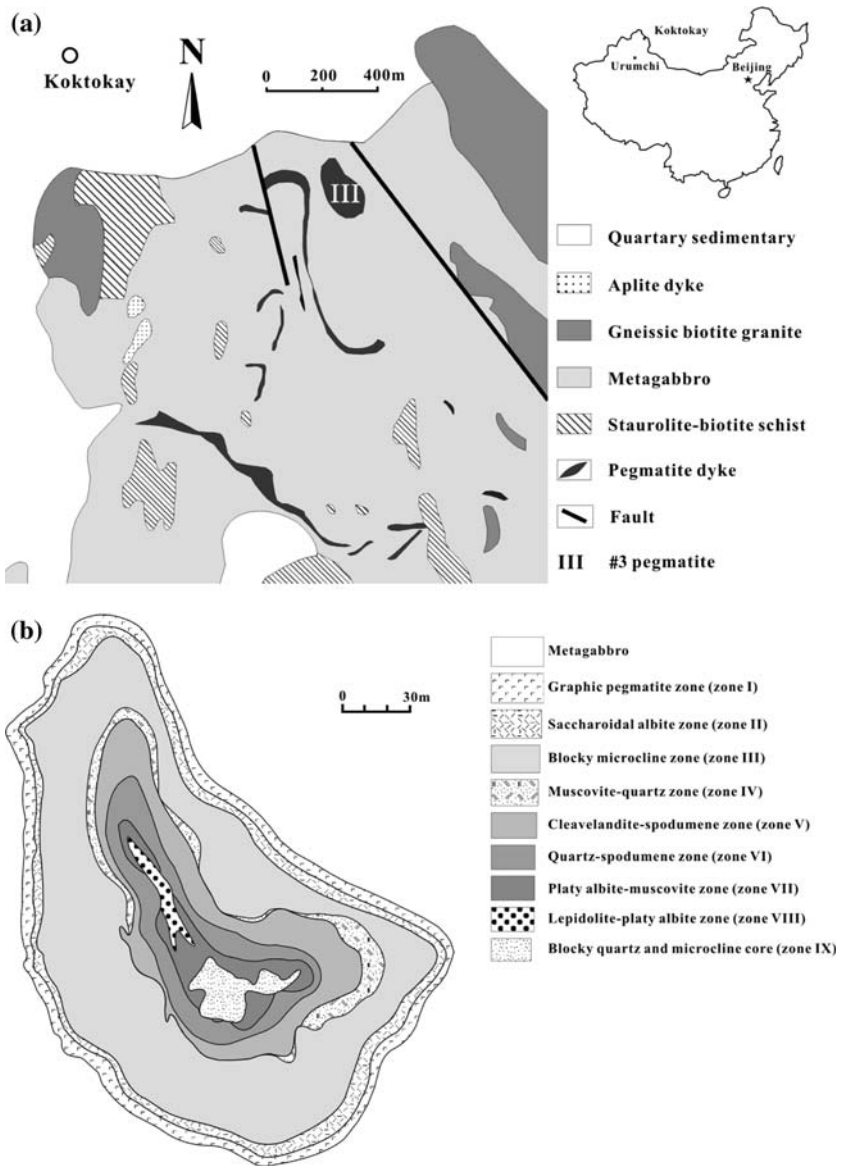

Fig. 1 Regional geological map (**a**) and internal textural zonation (**b**) of the Koktokay#3 granitic pegmatite, Altai, Northwestern China (modified after Wang et al. 1981; Zhu et al. 2000)

Results

Occurrence and composition of Cs-dominant lepidolite in the Koktokay#3 pegmatite

Micas (muscovite and lepidolite) occur as major constituents in most of the textural zones of the Koktokay#3 pegmatite. Four types of occurrence of the Cs-dominant lepidolite have been recognized in the inner pegmatite zones V–VIII.

Type A: Cs-dominant lepidolite as outer zone on lepidolite core

On a microscopic scale, abundant euhedral flakes of lepidolite are dispersed throughout the pollucite (Fig. 2a, b, c), but also form veinlets, up to 2 cm long, crosscutting the pollucite crystal (Fig. 2d, e, f). Flakes of lepidolite are between 100 and 200 μm wide and 200 μm to 2 mm long. They show zoning textures in BSE images, generally with a darker core (named Lep-A1 in Fig. 2a) and a brighter marginal zone (Lep-A2 in Fig. 2a) with a sharp boundary between them. Under the optical microscope, two types of zones can be distinguished by their interference colors in cross-polarized light (Fig. 2g, h). The cores are commonly narrow, down to 30 μm, whereas the outer zones are up to 150 μm wide. A narrow, almost complete rim of strongly Cs-rich pollucite (nearly the pollucite end-member, CRK > 90) [CRK = 100 × (Cs + K + Rb)/Σ(Cs + Na + K + Rb + Ca + Mg)] mostly 10–20 μm wide surrounds lepidolite inclusions in pollucite (CRK = 80–90).

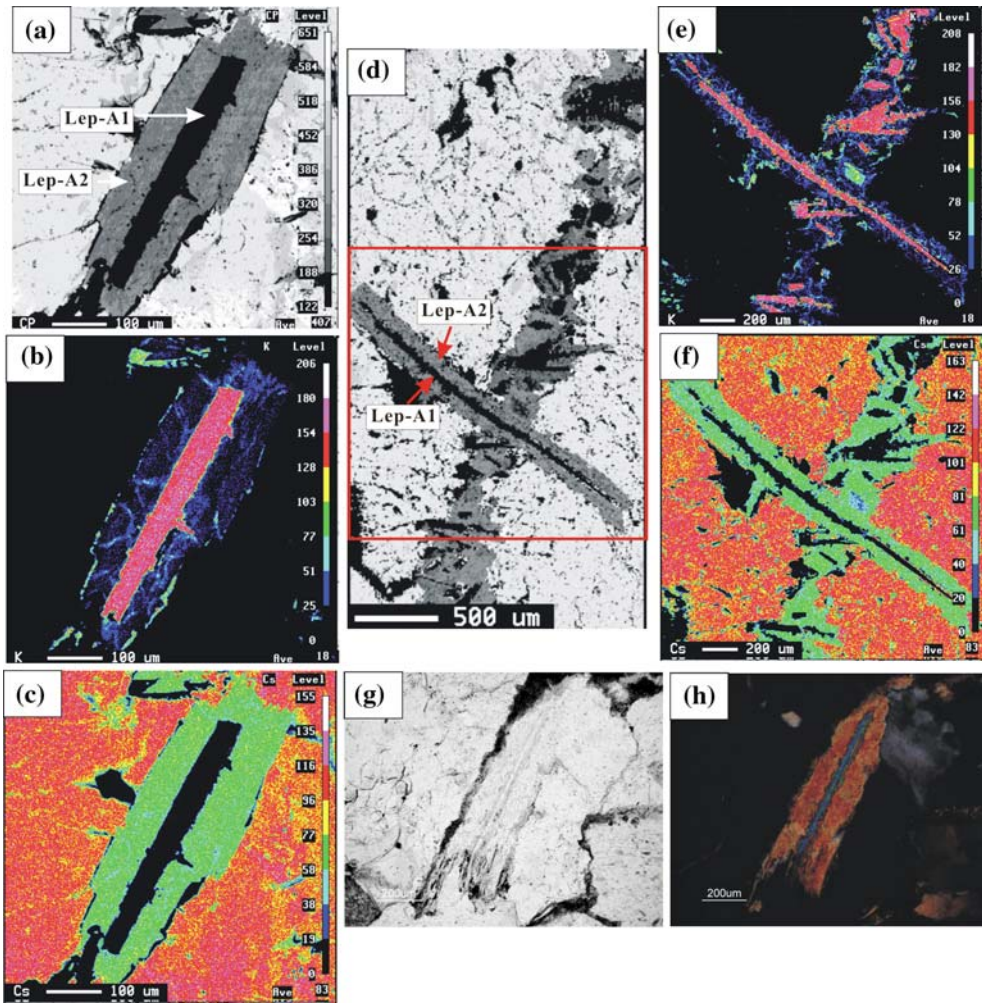

Fig. 2 Electron-microprobe maps and microphotograph of lepidolite (Lep-A1) and its outer Cs-rich zone (Lep-A2). **a–c** Zoned lepidolite flake enclosed in pollucite. **a** BSE image, **b–c** distribution maps of K and Cs, respectively; **d–f** veinlet of lepidolite crosscutting pollucite. **d** BSE, **e–f** distribution maps of the outlined area of K and Cs, respectively; **g–h** microphotograph of zoned lepidolite in pollucite. **g** Plane-polarized light, **h** cross-polarized light

X-ray compositional maps and quantitative EMP spot analyses of the lepidolite reveal strongly different K/Cs compositions between the core and outer zone, the latter being Cs-enriched (Fig. 2; Table 1). The Lep-A1 core is homogenous and contains on average 1.26 wt% Cs_2O. However, the homogenous marginal zones have Cs_2O of ~22.78 wt% ($1\sigma \pm 1.60$).

Type B: Cs-dominant lepidolite as finely-divided overgrowth on muscovite veinlets

In Fig. 3, adjacent to the pollucite crystal, a veinlet of muscovite (Mus-B1) is 2 mm long but only 10–20 μm thick. Microscopically, the muscovite is associated with small grains of tourmaline. Fine flakes of lepidolite (Lep-B1), overgrowing the muscovite, also form a veinlet with nearly the same thickness and length as the muscovite veinlet.

Compositionally, Lep-B1 corresponds to a Cs-dominant analog of polylithionite (Table 2). Muscovite is mostly homogeneous and close to the ideal formula (Table 2). Also, EMP analyses indicate that the associated tourmaline is rossmanite, an alkali-deficient species of the tourmaline group (Zhang et al. 2004a).

Type C: Cs-dominant lepidolite veinlets in rock-forming lepidolite

This type of Cs-enriched lepidolite is restricted to the lepidolite-platy albite zone VIII of the pegmatite.

Muscovite is the dominant mica in this zone. It forms coarse-grained finely-divided greenish to colourless aggregates (≤ 5 cm) locally associated with green elbaite, and overgrown by pink lepidolite. Masses of greenish muscovite show simple sharp boundaries against lepidolite. However, the lepidolite is microscopically strongly heterogeneous, as demonstrated both in a cross-polarized photomicrograph (Fig. 4a) and in a BSE image (Fig. 4b). Figure 4a shows that the rock-forming lepidolite (Lep-C1) encloses small muscovite flakes (Mus-C1). This is especially evident in the Al distribution map (Fig. 4e);

Table 1 Representative electron-microprobe compositions of micas (type A) from the Koktokay#3 pegmatite

Mica Abbr	Lep-A1			Lep-A2		
	P-3	S-7	Average (N = 15)	P-2	S-11	Average (N = 16)
SiO_2 (wt%)	54.12	52.40	53.59 (0.76)	48.18	47.55	47.63 (0.67)
Al_2O_3	20.60	22.47	21.84 (0.96)	16.89	16.05	16.78 (1.07)
FeO	0.00	0.07	0.02 (0.03)	0.00	0.03	0.03 (0.04)
MnO	0.10	0.12	0.11 (0.03)	0.06	0.09	0.13 (0.05)
MgO	0.00	0.00	0.00 (0.00)	0.01	0.00	0.02 (0.05)
Li_2O[a]	5.98	5.49	5.83 (0.22)	4.28	4.09	4.12 (0.19)
Na_2O	0.08	0.11	0.09 (0.02)	0.02	0.03	0.02 (0.03)
K_2O	11.00	10.94	10.97 (0.25)	2.12	1.00	1.90 (0.66)
Rb_2O	0.02	0.02	0.01 (0.01)	0.05	0.13	0.11 (0.02)
Cs_2O	1.26	1.53	1.26 (0.31)	22.46	25.06	22.78 (1.60)
CaO	0.00	0.00	0.00 (0.01)	0.00	0.03	0.02 (0.05)
F	6.63	6.63	6.71 (0.37)	5.17	5.77	5.35 (0.38)
Less F=O	2.78	2.79	2.82	2.17	2.43	2.25
H_2O[b]	1.33	1.30	1.32	1.39	1.02	1.27
Total	98.33	98.33	98.94	98.46	98.45	97.91
Si (*apfu*)	3.627	3.531	3.572	3.757	3.791	3.755
$Al^{(IV)}$	0.373	0.469	0.428	0.243	0.209	0.245
$Al^{(IV)}$	1.253	1.315	1.287	1.309	1.300	1.313
Fe	0.000	0.004	0.001	0.000	0.002	0.002
Mn	0.006	0.007	0.006	0.004	0.006	0.009
Mg	0.000	0.000	0.000	0.001	0.000	0.002
Li	1.612	1.487	1.562	1.341	1.313	1.306
	2.871	2.813	2.857	2.656	2.622	2.631
Na	0.011	0.014	0.012	0.003	0.005	0.003
K	0.940	0.940	0.933	0.211	0.102	0.190
Rb	0.001	0.001	0.000	0.003	0.007	0.005
Cs	0.036	0.044	0.036	0.746	0.851	0.766
Ca	0.000	0.000	0.000	0.000	0.003	0.002
	0.987	0.999	0.981	0.963	0.968	0.967
F	1.405	1.414	1.414	1.276	1.456	1.333
OH	0.595	0.586	0.586	0.724	0.544	0.667

Structural formulae are calculated on the basis of 11 atoms of O per formula unit (*apfu*)

N Number of electron-microbe analyses for average. See text for mica abbreviation

[a] Li_2O is estimated using the equation of Tindle and Webb (1990) for lepidolite, and that of Tischendorf et al. (1997) for muscovite

[b] H_2O values are calculated assuming the OH-F site is filled and amount of Cl is negligible

numerous Mus-1 inclusions vary from several to tens of microns. The rock-forming lepidolite Lep-C1 is mantled by optically and compositionally different lepidolite (Lep-C2). The mantle is 10–50 μm wide with a sharp outward transition into veinlets of Cs-rich lepidolite (Lep-C3), commonly several tens of microns wide. Overall, the veinlets appear as fillings along fissures or cleavages of the Lep-C1 lepidolite, forming parallel veinlets or networks. When albite is enclosed in lepidolite, Cs-lepidolite rims this mineral.

Electron-microprobe analyses have been carried out on all types of white mica present (Table 3). Muscovite approaches the end-member composition with very low Cs_2O content (Table 3). The average composition (wt%) of the rock-forming lepidolite classifies it as trilithionite (Table 3). The rim lepidolite (Lep-C2) is more silicic but less aluminous than Lep-C1, and may be considered a Cs-poor polylithionite (Table 3). The lepidolite veinlets (Lep-C3) are mostly homogenous- and Cs-rich, i.e., the Cs-dominant analog of polylithionite (Table 3).

Type D: Cs-dominant lepidolite as veinlets in elbaite

This type of Cs-dominant lepidolite forms veinlets cross-cutting tourmaline.

Associations of Cs-rich lepidolite with tourmaline are not common in the Koktokay#3 pegmatite. Very rarely, finely-divided Cs-rich lepidolite is enclosed in ''watermelon''-like tourmaline, associated with muscovite, quartz and pollucite (Zhang et al. 2006). Here we report veinlets of Cs-dominant lepidolite (Lep-D1) in a large pale pink crystal of elbaite, about 4 cm across (Fig. 5). The veinlets are sub-parallel, 100–150 μm thick and 100 μm to 2 mm long. Small flakes of muscovite (Mus-D1) are locally dispersed at the margins of the lepidolite veinlets. Lepidolite veinlets cross-cut different zones of elbaite, indicating a later formation.

The average EMP composition of Mus-D1 corresponds to end-member muscovite (Table 4). Cs-rich lepidolite Lep-D1 is mostly homogenous, and its composition indicates that it is the Cs analog of polylithionite (Table 4).

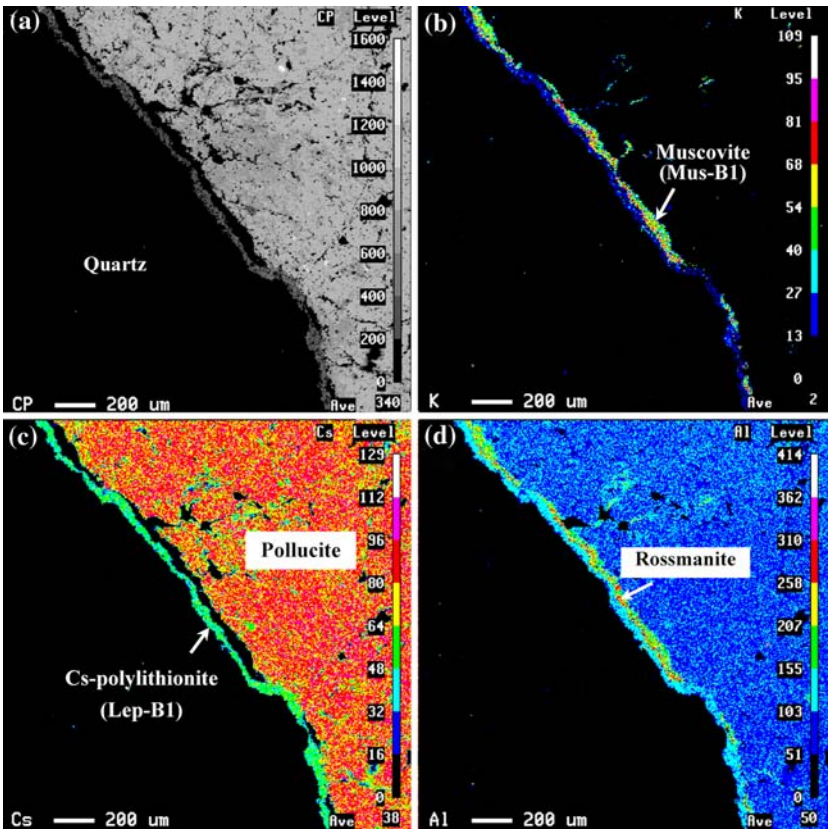

Fig. 3 Electron-microprobe maps of veinlet of muscovite + Cs-dominant polylithionite adjacent to a pollucite crystal. **a** BSE image; **c**–**d** distribution maps of K, Cs and Al

Structural character of the Cs-dominant lepidolite by in situ techniques

As shown above, Cs-rich lepidolite is always closely associated with normal lepidolite or muscovite. Therefore, it is impossible to separate physically Cs-dominant polylithionite to conduct routine X-ray diffraction analysis. For this reason, we chose micro-XRD and Raman probe to analyse the lepidolite in order to characterize the crystal structure of the Cs-dominant analog of polylithionite.

Micro-area X-ray diffraction

About 100-μm-sized micro-area X-ray diffraction was carried out on a polished thin section. We chose a zoned flake of lepidolite (the same type as lepidolite of type A, described in Sect. 4.1.1) about 500 μm wide, which is enclosed in pollucite. Figure 6 is the observed image of the section examined with a CCD camera. Electron-microprobe analyses revealed that the lepidolite core Lep1 contains 1.86 wt% Cs_2O [$(K_{0.84}Cs_{0.06}Rb_{0.01})_{0.91}(Al_{1.30}Li_{1.52})(Si_{3.66}Al_{0.34}O_{10})(OH)_{0.22}F_{1.78}$], whereas the outer zone Cs-Lep1 and Cs-Lep2 contain as much as 25.26 wt% Cs_2O [$(K_{0.11}Cs_{0.88})_{0.99}(Al_{1.46}Li_{1.00})(Si_{3.59}Al_{0.41}O_{10})(OH)_{0.54}F_{1.46}$]. The X-ray diffraction patterns of Lep1, Cs-Lep1 and Cs-Lep2 are shown in Fig. 7, and XRD data of a polylithionite [$K(Al_{0.62}Li_{1.30})(Si_{3.58}Al_{0.42}O_{10})(OH)_{0.485}F_{1.5}$] from the JCPDS catalog in the 2θ range of 0°–80° is given for comparison.

The X-ray diffraction patterns of the normal, Cs-poor lepidolite (Lep1 in Fig. 7) are characterized by several strong peaks [d in Å (I) (hkl): 2.983 (48) (025), 2.593 (38) (130), 1.506 (100) (–3.32), 1.014 (45) (446)], and are consistent with the standard patterns for polylithionite found in the JCPDS catalog. The diffraction patterns from two areas of the Cs-rich outer zone of lepidolite (Cs-Lep1 and Cs-Lep2, respectively, Fig. 7) are similar in terms of peak positions although their relative intensities are very different. Moreover, peak positions of the Cs-rich outer zone (Cs-Lep1) compare favorably with those of the polylithionite core (Lep1). Therefore, the similarity of XRD pattern of Cs-dominant polylithionite with that of the Cs-bearing polylithionite suggests that they are structural members of the lepidolite series. The cell parameters a, b, c (Å) and β (°) are 5.214, 9.100, 20.056, 99.571 for Lep1, 5.215, 9.066, 20.101, 99.559 for Cs-Lep1 and 5.218, 9.0597, 20.822, 99.1759 for Cs-Lep2, respectively. It is noted that the crystallographic results deduced from the micro-diffraction data must be treated with

Table 2 Representative electron-microprobe compositions of micas (type B) from the Koktokay#3 pegmatite

Mica Abbr	Lep-B1			Mus-B1		
	22	23	Average (N = 12)	11	19	Average (N = 10)
SiO_2 (wt%)	47.46	47.02	47.21 (1.13)	44.83	45.67	45.48 (0.34)
Al_2O_3	16.58	16.92	17.83 (0.71)	37.91	38.06	38.39 (0.34)
FeO	0.02	0.00	0.03 (0.03)	0.02	0.01	0.02 (0.03)
MnO	0.12	0.15	0.12 (0.04)	0.01	0.00	0.01 (0.01)
MgO	0.00	0.00	0.00 (0.01)	0.00	0.00	0.00 (0.00)
Li_2O^a	4.07	3.94	4.00 (0.33)	0.00	0.00	0.00 (0.00)
Na_2O	0.01	0.01	0.04 (0.03)	0.32	0.35	0.34 (0.03)
K_2O	0.60	0.63	1.72 (0.99)	11.09	11.01	11.04 (0.11)
Rb_2O	0.12	0.09	0.10 (0.02)	0.01	0.02	0.03 (0.04)
Cs_2O	25.93	25.61	23.14 (2.07)	0.28	0.30	0.25 (0.05)
CaO	0.02	0.00	0.02 (0.02)	0.03	0.00	0.01 (0.01)
F	4.95	5.40	5.34 (0.32)	0.00	0.00	0.00 (0.00)
Less F=O	2.08	2.27	2.24	0.00	0.00	0.00
H_2O^b	1.43	1.20	1.29	4.47	4.52	4.53
Total	99.22	98.69	98.66	98.96	99.95	100.13
Si (*apfu*)	3.769	3.750	3.700	3.003	3.025	3.007
$Al^{(IV)}$	0.231	0.250	0.300	0.997	0.975	0.993
$Al^{(IV)}$	1.320	1.342	1.347	1.997	1.996	1.999
Fe	0.001	0.000	0.002	0.001	0.000	0.001
Mn	0.008	0.010	0.008	0.000	0.000	0.000
Mg	0.000	0.000	0.000	0.000	0.000	0.000
Li	1.299	1.265	1.259	0.000	0.000	0.000
	2.629	2.616	2.616	1.998	1.997	2.001
Na	0.002	0.001	0.006	0.042	0.045	0.044
K	0.061	0.064	0.170	0.948	0.930	0.932
Rb	0.006	0.005	0.005	0.000	0.001	0.001
Cs	0.877	0.871	0.775	0.008	0.009	0.007
Ca	0.002	0.000	0.001	0.002	0.000	0.001
	0.948	0.940	0.958	1.000	0.984	0.985
F	1.244	1.361	1.324	0.000	0.000	0.000
OH	0.756	0.639	0.676	2.000	2.000	2.000

See the footnotes in Table 1 for processing of data

caution. Even so, the *c* parameter of Cs-rich lepidolite is larger than that of Cs-poor lepidolite, and this is probably related to the effect of incorporation of Cs^+ in the interlayer sites, as predicted from the cell parameter differences between nanpingite and muscovite (Yang et al. 1988; Ni and Hughes 1995).

Micro-Raman spectra

The zoned crystal of lepidolite shown in Fig. 7 was also studied by micro-Raman spectrometry in order to compare Cs-dominant polylithionite with a Cs-bearing lepidolite-series mineral.

The Raman spectra of the Cs-bearing core (as Lep-A1) and Cs-rich rim (as Lep-A2) of the lepidolite are very similar in their peak positions. Raman peaks were assigned on the basis of previous results of McKeown et al. (1999a, b) and Wang et al. (2002). The peak at about 1,150 cm^{-1} is attributed to the stretching mode of the Si–O_{nb} bond (O_{nb}: non-bridging oxygen) in SiO_4 tetrahedra. The typical peak for phyllosilicate minerals at ~700 cm^{-1} is well displayed for both the conventional lepidolite and the Cs-dominant lepidolite, corresponding to both Si–O stretching and O–Si–O bending deformations (Wang et al. 2002). The Raman peaks in the <600 cm^{-1} region arise from a complex set of translational motions of cations in octahedral and interlayer sites relative to the SiO_4 groups, oxygen atoms and OH groups (including their transitional and vibrational motions).

Discussion

Compositional variations across different paragenetic types of lepidolite

Our studies show that there is a broad range of alkali contents in the lepidolite, and that a good inverse correlation exists between K and Cs in the series between lepidolite and Cs-rich lepidolite (Fig. 8). Rb, Na and Ca contents in the alkali site are low.

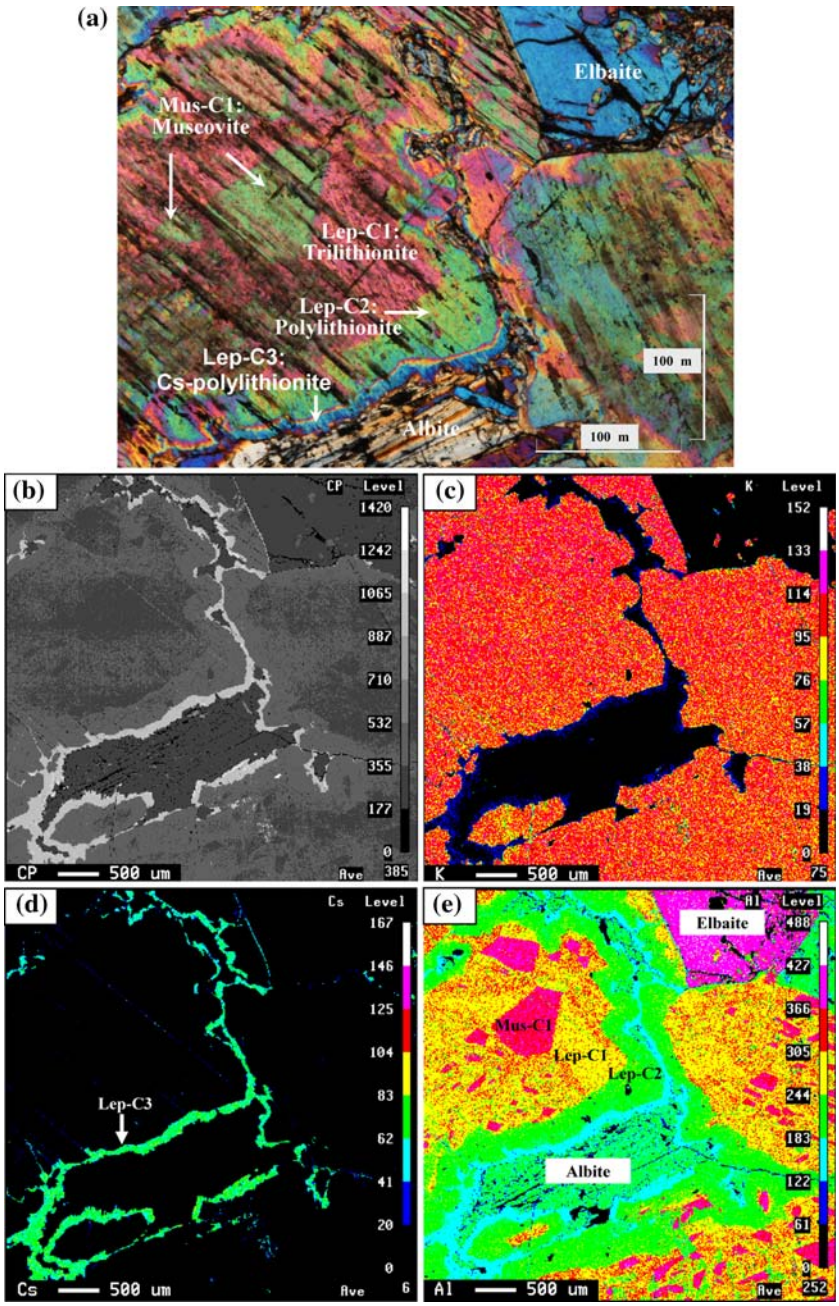

Fig. 4 Photomicrograph (**a**) and electron-microprobe maps (**b–e**) of aggregate of different lepidolites (Lep-C1, Lep-C2, Lep-C3) and muscovite (Mus-C1). **b** BSE image; **c–e** distribution maps of K, Cs and Al

A plot of ^{IV}Al versus Cs/(K + Cs) (Wang et al. 2004) separates the data into three sub-groups. Lep-C1 lepidolite has a Cs/(K + Cs) value less than 0.1, with ^{IV}Al values of around 0.8, corresponding to trilithionite. The Cs/(K + Cs) ratios of Lep-A1 and Lep-C2 are below 0.10, with ^{IV}Al from 0.37 to 0.58, mostly in the polylithionite range. Compositions of Lep-A2, Lep-B1, Lep-C3 and Lep-D1 have ^{IV}Al between 0.11 and 0.37 and Cs/(K + Cs) from 0.61 to 0.92, thus corresponding to a Cs-dominant analog of polylithionite.

Evidence for dominance of Cs in some types of lepidolite is given by Černý et al. (2003) and also this study. However, Wang et al. (2004) have demonstrated in lepidolites from the Yichun topaz–lepidolite granite that Cs enrichment occurs only in polylithionite. In this study also there is virtually no Cs enrichment in trilithionite (Fig. 9), only polylithionite exhibits Cs enrichment. There is no evidence for the existence of a Cs-dominant analog of trilithionite.

Late mobility of Cs in the Koktokay#3 pegmatite

Cesium is an incompatible element that is progressively enriched in the melt with advancing crystallization.

Table 3 Representative electron-microprobe compositions of micas (type C) from the Koktokay#3 pegmatite

Mica Abbr	Mus-C1			Lep-C1			Lep-C2			Lep-C3		
	21	22	Average (N = 13)	43	47	Average (N = 11)	4	16	Average (N = 17)	8	27	Average (N = 16)
SiO_2 (wt%)	45.99	45.16	45.51 (0.76)	49.11	48.21	48.72 (0.65)	51.56	53.28	52.88 (1.06)	47.17	47.62	47.45 (0.62)
Al_2O_3	36.76	36.74	36.76 (1.92)	29.28	28.26	29.16 (0.73)	24.83	21.76	22.53 (1.06)	17.08	17.43	17.06 (0.96)
FeO	0.11	0.09	0.08 (0.05)	0.05	0.12	0.13 (0.06)	0.12	0.20	0.14 (0.05)	0.11	0.11	0.10 (0.06)
MnO	0.13	0.08	0.12(0.08)	0.21	0.26	0.28 (0.13)	0.38	0.35	0.30 (0.08)	0.30	0.27	0.22 (0.07)
MgO	0.00	0.00	0.00 (0.00)	0.00	0.00	0.00 (0.00)	0.00	0.00	0.00 (0.00)	0.00	0.00	0.00 (0.00)
Li_2O[a]	0.51	0.32	0.76 (1.03)	4.54	4.28	4.43 (0.19)	5.25	5.74	5.62 (0.30)	3.99	4.11	4.07 (0.18)
Na_2O	0.33	0.28	0.37 (0.07)	0.30	0.28	0.24 (0.08)	0.16	0.11	0.13 (0.04)	0.00	0.05	0.02 (0.01)
K_2O	10.67	10.95	10.95 (0.19)	11.06	11.18	11.02 (0.26)	11.44	11.19	11.08 (0.22)	1.72	2.39	2.12 (0.45)
Rb_2O	0.08	0.12	0.04 (0.04)	0.00	0.01	0.05 (0.05)	0.07	0.02	0.04 (0.03)	0.09	0.07	0.08 (0.04)
Cs_2O	0.09	0.08	0.08 (0.04)	0.16	0.22	0.20 (0.07)	0.24	0.95	0.86 (0.37)	23.29	22.18	22.77 (0.89)
CaO	0.02	0.00	0.02 (0.01)	0.02	0.00	0.02 (0.02)	0.02	0.01	0.01 (0.01)	0.00	0.01	0.01 (0.02)
F	1.22	0.86	1.30 (0.63)	3.13	4.10	4.02 (0.72)	5.32	7.30	6.29 (0.91)	5.63	5.44	5.40 (0.35)
Less F=O	0.51	0.36	0.55	1.31	1.72	1.69	2.24	3.06	2.64	2.37	2.29	2.27
H_2O[b]	3.93	4.05	3.88	3.06	2.49	2.61	1.99	1.03	1.51	1.12	1.26	1.25
Total	99.37	98.45	99.37	99.68	97.69	99.21	99.13	98.93	98.78	98.14	98.66	98.31
Si (*apfu*)	3.055	3.036	3.029	3.236	3.256	3.233	3.424	3.557	3.529	3.730	3.713	3.732
$Al^{(IV)}$	0.945	0.964	0.971	0.764	0.744	0.767	0.576	0.443	0.471	0.270	0.287	0.268
$Al^{(IV)}$	1.933	1.947	1.913	1.511	1.506	1.514	1.368	1.269	1.301	1.323	1.316	1.312
Fe	0.006	0.005	0.005	0.002	0.007	0.007	0.007	0.011	0.008	0.007	0.007	0.007
Mn	0.007	0.004	0.007	0.012	0.015	0.016	0.021	0.020	0.017	0.020	0.018	0.015
Mg	0.000	0.000	0.000	0.000	0.000	0.000	0.000	0.000	0.000	0.000	0.000	0.000
Li	0.137	0.087	0.205	1.204	1.164	1.182	1.401	1.541	1.509	1.268	1.290	1.286
	2.083	2.043	2.129	2.729	2.691	2.719	2.797	2.841	2.835	2.618	2.631	2.620
Na	0.042	0.036	0.048	0.038	0.037	0.031	0.021	0.014	0.017	0.000	0.007	0.003
K	0.904	0.939	0.930	0.930	0.964	0.933	0.969	0.953	0.943	0.174	0.238	0.213
Rb	0.003	0.005	0.002	0.000	0.000	0.002	0.003	0.001	0.002	0.005	0.004	0.004
Cs	0.002	0.002	0.002	0.004	0.006	0.006	0.007	0.027	0.025	0.785	0.737	0.763
Ca	0.002	0.000	0.001	0.002	0.000	0.001	0.001	0.001	0.000	0.000	0.001	0.001
	0.954	0.983	0.983	0.974	1.007	0.973	1.000	0.996	0.987	0.963	0.986	0.985
F	0.257	0.183	0.273	0.652	0.877	0.845	1.118	1.540	1.327	1.408	1.342	1.344
OH	1.743	1.817	1.727	1.348	1.123	0.673	0.882	0.460	0.656	0.592	0.658	0.655

See the footnotes in Table 1 for processing of data

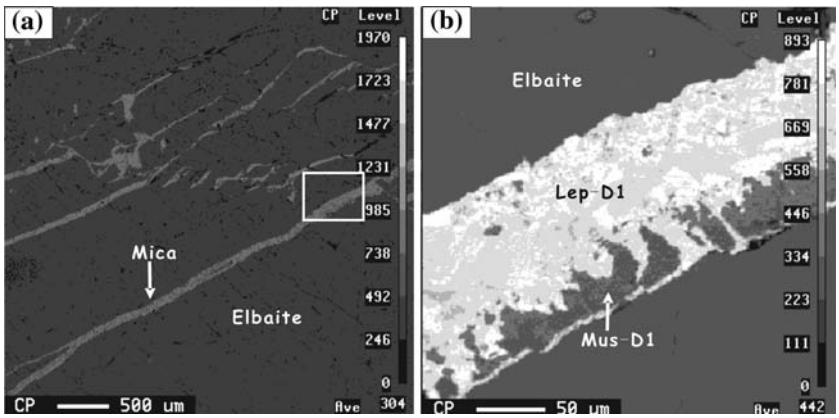

Fig. 5 Backscattered electron images of sub-parallel veinlets of Cs-dominant polylithionite (Lep-D1) rimmed by muscovite (Mus-D1) in elbaite crystal. Outlined area in (**a**) is enlarged as shown in (**b**)

In the Koktokay#3 pegmatite, Cs enrichment is most pronounced in the inner zones V–VIII, where primary pollucite crystallized as the major Cs phase under near-solidus transitional stages from magmatic to hydrothermal conditions (Wang et al. 2006). Late mobility of Cs is also found in lepidolite but only in later generations that overgrow, rim or vein the primary rock-forming lepidolite. The formation of cesian end-

Table 4 Representative electron-microprobe compositions of micas (type D) from the Koktokay#3 pegmatite

Mica Abbr	Lep-D1			Mus-D1		
	1	6	Average (N = 15)	13	18	Average (N = 7)
SiO_2 (wt%)	46.25	47.94	47.12 (0.86)	44.57	45.24	44.93 (0.31)
Al_2O_3	17.08	15.26	16.93 (0.84)	37.68	37.39	37.77 (0.48)
FeO	0.10	0.05	0.07 (0.06)	0.00	0.09	0.04 (0.03)
MnO	0.16	0.14	0.14 (0.03)	0.02	0.03	0.03 (0.02)
MgO	0.00	0.00	0.00 (0.00)	0.00	0.00	0.00 (0.00)
Li_2O[a]	3.72	4.21	3.97 (0.25)	0.00	0.00	0.00 (0.00)
Na_2O	0.03	0.04	0.02 (0.02)	0.61	0.23	0.31 (0.14)
K_2O	0.89	0.85	1.38 (0.50)	10.47	10.97	10.89 (0.19)
Rb_2O	0.09	0.12	0.11 (0.02)	0.01	0.02	0.01 (0.01)
Cs_2O	26.09	24.34	24.52 (1.27)	0.20	0.29	0.25 (0.07)
CaO	0.00	0.03	0.01 (0.01)	0.02	0.02	0.01 (0.01)
F	4.70	5.67	4.96 (0.29)	0.00	0.00	0.00 (0.00)
Less F=O	1.97	2.38	1.69	0.01	0.01	0.00
H_2O[b]	1.50	1.06	1.42	4.44	4.47	4.47
Total	98.64	97.39	98.59	98.03	98.76	98.70
Si (*apfu*)	3.722	3.836	3.740	3.006	3.033	3.013
$Al^{(IV)}$	0.278	0.164	0.260	0.994	0.967	0.987
$Al^{(IV)}$	1.343	1.275	1.323	2.001	1.987	1.998
Fe	0.007	0.003	0.005	0.000	0.005	0.002
Mn	0.011	0.010	0.010	0.001	0.002	0.002
Mg	0.000	0.000	0.000	0.000	0.000	0.000
Li	1.205	1.354	1.267	0.000	0.000	0.000
	2.565	2.642	2.605	2.002	1.994	2.002
Na	0.004	0.005	0.004	0.080	0.030	0.041
K	0.092	0.087	0.139	0.901	0.938	0.931
Rb	0.005	0.006	0.005	0.000	0.001	0.000
Cs	0.895	0.830	0.830	0.006	0.008	0.007
Ca	0.000	0.003	0.001	0.001	0.002	0.001
	0.995	0.931	0.979	0.988	0.979	0.981
F	1.196	1.434	1.247	0.000	0.000	0.000
OH	0.804	0.566	0.753	2.000	2.000	2.000

See the footnotes in Table 1 for processing of data

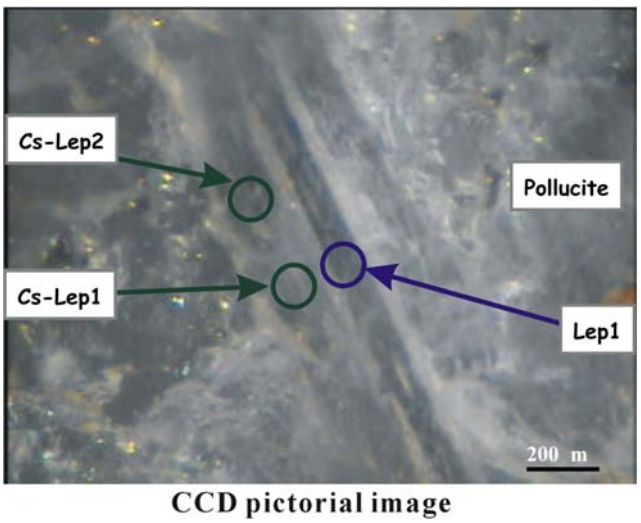

Fig. 6 CCD image of lepidolite for micro-XRD measurement. *Color circles* indicate location of micro-XRD measurement

members of micas is thus linked to hydrothermal Cs-rich solutions circulating in the internal zones of the pegmatite (Lagache 1995).

Fluid-melt partition coefficients for Cs published by Webster et al. (1989) are variable, but they can be expected to increase as temperature decreases. In fact, the Cs contents in magmatic fluids should increase with progressive crystallization of granitic magma (Audétat and Pettke 2003). The fact that pollucite and nanpingite-like mica occur as cavity phases in the lithium pegmatite of the O'Grady batholith (Ercit et al. 2003) also indicates that Cs enrichment in fluid is likely. In the case of the Koktokay#3 pegmatite, Cs-bearing fluids may have exsolved during the evolution of the pegmatitic magma. This type of fluid replaced early-formed lepidolite along margins, leading to the formation of Cs-dominant polylithionite as outer zones on primary lepidolite. On the other hand, Cs-dominant

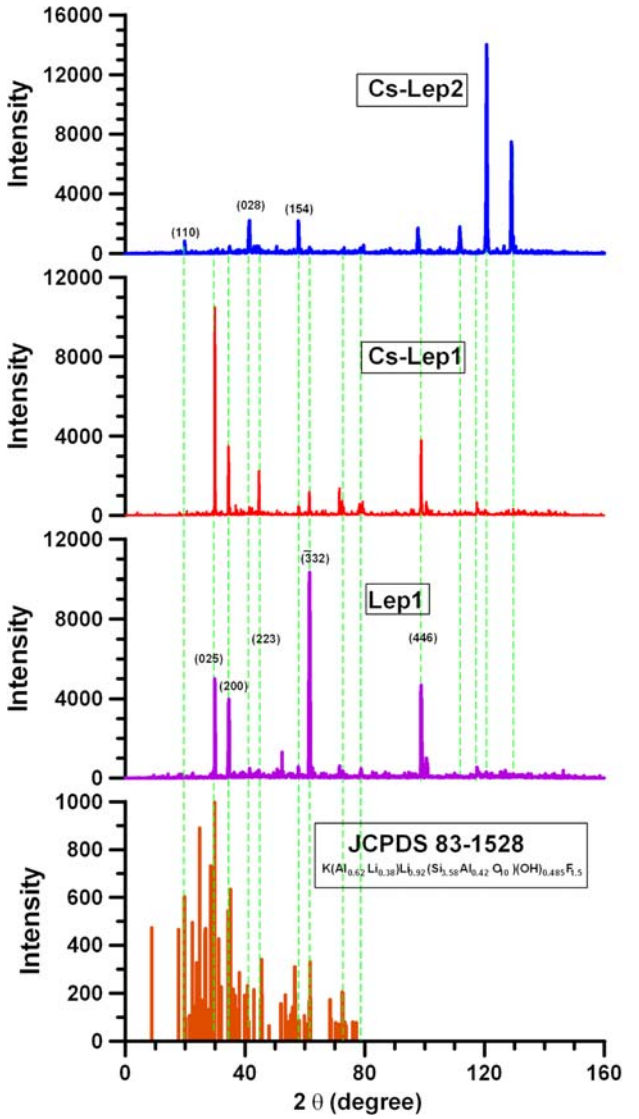

Fig. 7 Micro-area XRD patterns of zoned lepidolite in Fig. 6, in comparison with the reference pattern of polylithionite (JCPDS 83-1528)

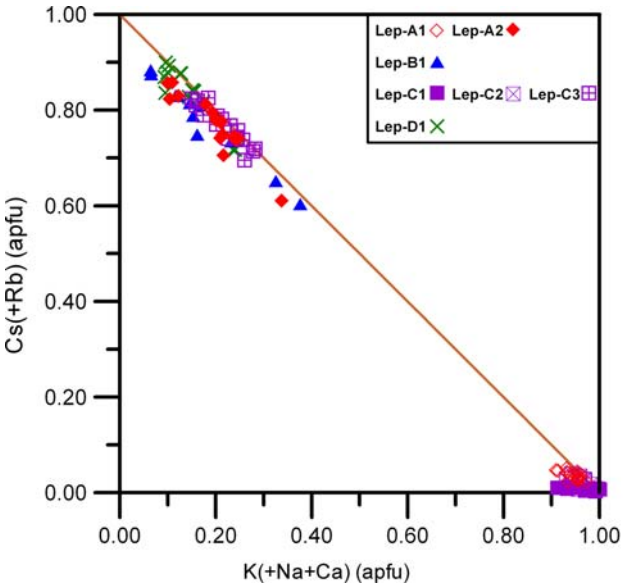

Fig. 8 Plots of concentrations of K(+Na+Ca) versus Cs(+Rb)(atomic values) in the lepidolite, with concentrations expressed in atoms per formula unit, *apfu*

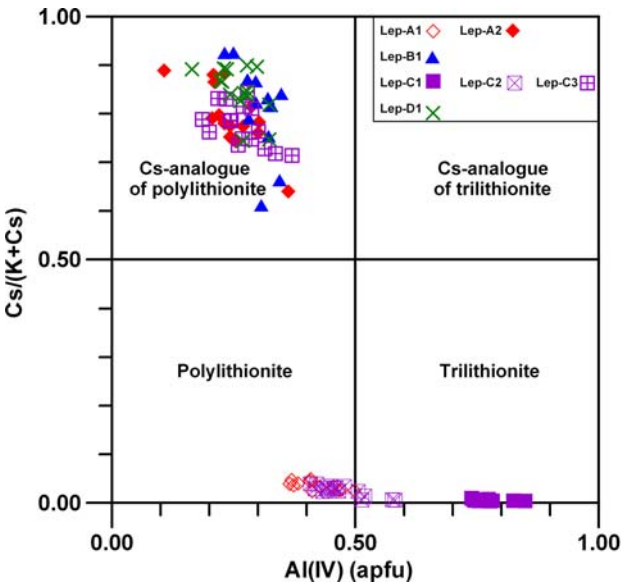

Fig. 9 Plots of compositions of lepidolite from the Koktokay#3 pegmatite in terms of ^{IV}Al (*apfu*) versus atomic Cs/(K + Cs). See text for abbreviations of lepidolite symbols

polylithionite may also have precipitated from Cs-rich fluids together with muscovite (Fig. 3).

Implications for the storage of radioactive cesium

^{137}Cs is a highly radioactive fission product from the irradiation of nuclear fuels, and a major radioactive component of high-level waste (HLW). Because of its large ionic radius (1.67 Å, Shannon 1976), only very few inorganic structures are capable of strongly fixing it. Thus, natural Cs-bearing minerals, especially pollucite ($CsAlSi_2O_6$), have been considered and investigated for storing nuclear materials (Černý 1979; Teertstra and Černý 1992). However, the wide variety of alteration products that can replace natural pollucite (e.g., Teertstra et al. 1992; Wang et al. 2006) indicate its instability under diverse conditions. Two synthetic mica-like phases, ''Cs-annite'' and ''Cs-tetra-ferri-annite'', have been recently synthesized and structurally characterized (Mellini et al. 1996; Drábek et al. 1998; Comodi et al. 1999) and offer alternatives for

efficiently immobilizing radioactive Cs. Thus, Cs-dominant lepidolite found in granitic environments (Černý et al. 2003; Wang et al. 2004; this study) may thus be a potential candidate for the immobilization of radioactive cesium waste:

1. Cesium retaining capacity of storing nuclear materials is important for immobilization of Cs. Klika et al. (2006) indicated that synthetic mica ''Cs-tetra-ferri-annite'' has limited Cs leachability. This phase has demonstrated a high degree of Cs retention as a function of pH and over temperatures from ambient to 100°C. In the natural pegmatite system, the migration and dispersal of Cs increases with decreasing temperature (Teertstra and Černý 1997). Overall, the evolution of Cs ended when it became incorporated into lepidolite under low-temperature hydrothermal conditions in the Altai pegmatite. As the Cs-dominant lepidolite has not been altered after its formation, it retains its Cs content.
2. To prevent Cs dispersal from underground HLW repositories it may be necessary to use material that can sorb Cs from infiltrating contaminated water. Micas, as one type of sheet silicate, are a common component of engineered barrier materials (Wang et al. 1998) because they strongly absorb Cs^+ with little desorption under natural conditions. The present study indicates that natural lepidolite can accommodate significant quantities of Cs in the interlayer sites. As lepidolite naturally occurs in granitic rocks, this type of rocks may control immobilization and transport of radionuclide cesium in underground water solutions, and is considered to be important host-rocks of geological disposal sites of high-level radwastes.
3. The synthesis of ''Cs-tetra-ferri-annite'' is controlled by temperature, pressure and particularly oxygen fugacity. However, the formation of Cs-dominant lepidolite is mainly related to hydrothermal conditions, either as a consequence of replacement of non Cs-bearing lepidolite by Cs-rich fluids through $K \Longleftrightarrow Cs$ substitution, or as a direct precipitation from Cs-rich fluids. In the virtual absence of Fe, the influence of oxygen fugacity would be negligible in the synthesis of Cs-dominant lepidolite.
4. Nanpingite, the Cs analog of muscovite, has never been reported other than from its type locality. The coexistence of Cs-poor muscovite with Cs-rich lepidolite in the Altai pegmatite indicates preferential partitioning of Cs into lepidolite.
5. Before Cs-lepidolite can be adopted as a repository mineral for Cs in nuclear waste, precise data on the temperature and pressure controls of its formation need to be determined. Detailed studies under a variety of physical and chemical conditions are also necessary to better understand the behavior of Cs-dominant lepidolite in aqueous solutions. Perhaps most importantly, further work to establish the radiation stability and long-term durability of Cs-rich micas are required.

Conclusions

Cesium may be the dominant cation in inter-layer sites of lepidolite, with Cs_2O ranging up to 21–26 wt%. Characterizations of the Koktokay#3 pegmatite samples using in situ techniques (micro-XRD and micro-Raman) revealed that Cs-dominant polylithionite structurally belongs to minerals of the lepidolite series. The Cs-dominant analog of polylithionite has been described (Red Cross Lake pegmatite, Canada, Černý et al. 2003; Yichun lepidolite–topaz granite, China, Wang et al. 2004; Haapaluoma and Viitaniemi pegmatites, Finland, Vîzná, Czech Republic, and Å kerberg, Sweden, P. Černý 2006, personal communication). The present study confirms the natural occurrence of ''cesium lepidolite'', although the data are not sufficient for a formal proposal to the International Mineralogical Association. Thus, nanpingite remains the only officially recognized mica species with dominant Cs.

Cs-dominant lepidolite in the Koktokay pegmatite was formed by replacement of lepidolite by, or by direct precipitation from, hydrothermal Cs-enriched fluids. This Cs- rich species has not been altered suggesting that Cs-rich lepidolite could be used as a repository of radioactive cesium waste.

Acknowledgments This paper benefited from critical comments of P. Černý, J. Hoefs and another anonymous reviewer. Their careful comments and helpful suggestions improved greatly the manuscript. The authors would like to thank Rodney Grapes who improved the manuscript from scientific and English grounds. Financial support for this work was provided by NSF of China grants 40221301, 40302010 and 40025209. Additional support was received from a joint China–France cooperative program PRA T02-03.

References

Armstrong JT (1989) CITZAF: combined ZAF and phirho(Z) electron beam correction programs. California Institute of Technology, Pasadena, California

Audétat A, Pettke T (2003) The magmatic-hydrothermal evolution of two barren granites: a melt and fluid inclusion study

of the Rito del Medio and Cañada Pinabete plutons in northern New Mexico (USA). Geochim Cosmochim Acta 67:97–121

Černý P (1979) Pollucite and its alteration in geological occurrences and in deep-burial radioactive waste disposal. In: GI McCarthy (ed) Scientific basis for Nuclear Waste Management, 1, 231–236, Prenum Press, New York

Černý P (1991) Rare-element granitic pegmatites. I. Anatomy and internal evolution of pegmatite deposits. Geosci Can 18:49–67

Černý P, Teertstra DK, Chapman R, Fryer BJ, Longstaffe FJ, Wang X-J, Chackowsky LE, Meintzer RE (1994) Mineralogy of extreme fractionation in rare-element granitic pegmatites at Red Cross Lake, Manitoba, Canada. IMA, 16th General Meeting, Pisa, Abstracts, 67

Černý P, Chapman R, Teertstra DK, Novák M (2003) Rubidium- and cesium-dominant micas in granitic pegmatites. Am Mineral 88:1832–1835

Comodi P, Zanazzi PF, Weiss Z, Rieder M, Drábek M (1999) ''Cs-tetra-ferri-annite:'' High-pressure and high-temperature behavior of a potential nuclear waste disposal phase. Am Mineral 84:325–332

Drábek M, Rieder M, Viti C, Weiss Z, Frýda J (1998) Hydrothermal synthesis of a Cs ferruginous trioctahedral mica. Can Mineral 36:755–761

Ercit TS, Groat LA, Gault RA (2003) Granitic pegmatites of the O'Grady batholith, N.W.T., Canada: A case study of the evolution of the elbaite subtype of rare-element granitic pegmatite. Can Mineral 41:117–137

Ginsburg AI, Lugovskoi GP, Ryabenko VE (1972) Cesian mica – a new type of mineralization. Geol Mineral Res 8:1–7 (in Russian)

Hawthorne FC, Teertstra DK, Černý P (1999) Crystal-structure refinement of a rubidian cesian phlogopite. Am Mineral 84:778–781

Huang XL, Wang RC, Chen XM, Hu H, Liu CS (2002) Vertical variations in the mineralogy of the Yichun topaz-lepidolite granite, Jiangxi Province, southern China. Can Mineral 40:1047–1068

Klika Z, Weiss Z, Mellini M, Drabek M (2006) Water leaching of cesium from selected cesium mineral analogues. Appl Geochem 21(3):405–418

Lagache M (1995) New experimental data on the stability of the pollucite-analcime series: application to natural assemblages. Eur J Mineral 7:319–323

McDonough WF, Sun SS, Ringwood AE, Jagoutz E, Hofmann AW (1992) Potassium, rubidium and cesium in the Earth and Moon and the evolution of the mantle of the Earth. Geochim Cosmochim Acta 56:1001–1012

McKeown DA, Bell MI, Etz ES (1999a) Raman spectra and vibrational analysis of the trioctahedral mica phlogopite. Am Mineral 84:970–976

McKeown DA, Bell MI, Etz ES (1999b) Vibrational analysis of the dioctahedral mica: 2M1 muscovite. Am Mineral 84:1041–1048

Mellini M, Weiss Z, Rieder M, Drábek M (1996) Cs-ferriannite as a possible host for waste cesium: crystal structure and synthesis. Eur J Mineral 8:1265–1271

Rigaku Corporation (1999) D/max-RAPID: Fast X-ray diffractometer with area detector. Rigaku J 16(2):1–7

Shannon RD (1976) Revised effective ionic radii and systematic studies of interatomic distances in halides and chalcogenides. Acta Crystallogr A32:751–767

Teertstra DK, Černý P (1992) Controls on morphology of analcime-pollucite in natural minerals, synthetic phases, and nuclear waste products. Crystal Res Techn 27:931–939

Teertstra DK, Černý P (1997) The compostional evolution of pollucite from African granitic pegmatites. J African Earth Sciences 25:317–331

Teertstra DK, Černý P, Chapman R (1992) Compositional heterogeneity and alteration of pollucite from High Grade Dyke, southeastern Manitoba. Can Mineral 30:687–697

Tindle AG, Webb PC (1990) Estimation of lithium contents in trioctahedral micas using microprobe data: application to micas from granitic rocks. Eur J Mineral 2:595–610

Tischendorf G, Gottesmann B, Förster HJ, Trumbull RB (1997) On Li-bearing micas: estimating Li from electron microprobe analyses and an improved diagram for graphical representation. Mineral Mag 61:809–834

Wang XJ, Zou TR, Xu JG, Yu XY, Qiu YZ (1981) Study of pegmatite minerals of the Altai region. Science Publishing House, Beijing, China (in Chinese)

Wang LM, Wang SX, Gong WL, Ewing RC (1998) Temperature dependence of Kr ion-induced amorphization of mica minerals. Nucl Instr and Meth B 141:501–508

Wang A, Freeman J, Kuebler KE (2002) Raman spectroscopic characterization of phyllosilicates. Lunar Planet Sci XXXIII, http://www.es.lancs.ac.uk/psrg/abstract/2002

Wang RC, Hu H, Zhang AC, Huang XL, Ni P (2004) Pollucite and the cesium-dominant analogue of polylithionite as expressions of extreme Cs enrichment in the Yichun topaz-lepidolite granite, southern China. Can Mineral 42:883–896

Wang RC, Hu H, Zhang AC, Fontan F, Zhang H, de Parseval Ph (2006) Occurrence and late re-equilibration of pollucite from the Koktokay no.3 pegmatite, Altai, northwestern China. Am Mineral 91:729–739

Webster JD, Holloway JR, Hervig RL (1989) Partitioning of lithophile trace elements between H_2O and H_2O + CO_2 fluids and topaz rhyolite melt. Econ Geol 84:116–134

Yang YQ, Ni YX, Wang LB, Wang WY, Zhang YP, Chen CH (1988) Nanpingite—a new cesium mineral. Acta Petrol Mineral Sinica, 7, 49–58 (in Chinese with English abstract)

Zhang AC, Wang RC, Hu H, Chen XM, Zhang H (2004a) Occurrences of foitite and rossmanite from the Koktokay No.3 granitic pegmatite dyke, Altai, northwestern China: A record of hydrothermal fluids. Can Mineral 42:873–882

Zhang AC, Wang RC, Hu H, Zhang H, Zhu JC, Chen XM (2004b) Chemical evolution of Nb-Ta oxides and zircon from the Koktokay No. 3 granitic pegmatite, Altai, northwestern China. Mineral Mag 68:739–756

Zhang AC, Wang RC, Zhang H, Hu H, Jiang SY (2006) Compositional evolution and significance of tourmaline from the Koktokay No.3 granitic pegmatite, Altai, Northwestern China. Can Mineral (submitted)

Zhu JC, Wu CN, Liu CS, Li FC, Huang XL, Zhou DS (2000) Magmatic-hydrothermal evolution and genesis of Koktokay No.3 rare metal pegmatite dyke, Altai, China. Geol J China Univ 6(1):40–52 (in Chinese with English abstract)